*Aerosol and Air Quality Research*, 16: 2186–2197, 2016

ISSN: 1680-8584 print / 2071-1409 online
doi: 10.4209/aaqr.2016.06.0280

# Effect of Operating Conditions on PAHs Emission from a Single $H_2$-$O_2$ PEM Fuel Cell

**Kuo-Lin Huang[1*], Ming-Sheng Wu[1], Jen-Hsiung Tsai[1], Ding-Yan Lin[1], Shui-Jen Chen[1], Wen-Jhy Lee[2]**

[1] *Department of Environmental Engineering and Science, National Pingtung University of Science and Technology, Neipu, Pingtung 91201, Taiwan*
[2] *Department of Environmental Engineering, National Cheng Kung University, Tainan City 70101, Taiwan*

## ABSTRACT

This study investigates the emissions of polycyclic aromatic hydrocarbons (PAHs) from a single hydrogen-oxygen proton exchange membrane (PEM) fuel cell (FC) under different flowrates, temperatures, sampling periods, and membrane-electrode assemblies (MEAs). The results show that Nap, PA, BeP, FL, Pyr, BbC, Ant, and Flu were dominant in anode and cathode emissions of the single PEMFC under different operating conditions. The emission concentrations of Total-PAHs and Total-BaP equivalent carcinogenic potency ($BaP_{eq}$) were lower from the anode than from the cathode emission. Moreover, the concentrations of molecular-weight (MW) classified PAHs were in the order low (L) MM- > high (H) MW- > middle (M) MW-PAHs. When the anode/cathode gas flowrates were greater or smaller than 52/35 sccm but at the same sampling volume, the emission concentrations of Total-PAHs and Total-$BaP_{eq}$ increased. The concentration of Total-PAHs decreased but the mass of Total-PAHs increased with the increase of sampling time. However, 64% and 82% of PAH mass were emitted within 12 and 24 h, respectively, based on 36 h sampling at anode/cathode gas flowrates = 52/35 sccm. The concentrations of Total-PAHs or Total-$BaP_{eq}$ of anode or cathode emission were slightly higher at 90°C than at 65°C.

The performances of commercial MEAs were in the order SGL < E-TEK < GORE. Nevertheless, the concentrations of anode or cathode emission Total-PAHs or Total-$BaP_{eq}$ for the PEMFC using different MEAs followed the order GORE > E-TEK2 > E-TEK > SGL, while the sums of anode and cathode Total-PAHs emission factors varied with the order SGL > E-TEK > E-TEK2 > GORE (13.3 ± 0.55, 11.5 ± 0.21, 7.91 ± 0.47, and 3.17 ± 0.22 μg $g^{-1}$-MEA, respectively). When using the (lab-made) E-TEK2 as the MEA of PEMFC, the PAH profiles of anode and cathode emission gases were similar to those of some carbon materials.

***Keywords:*** Polycyclic aromatic hydrocarbon; Proton exchange membrane fuel cell; Emission factor.

## INTRODUCTION

Polycyclic aromatic hydrocarbons (PAHs) (particularly benzo[a] pyrene (BaP)) have been a concern for their adverse health effects (Lin *et al.*, 2008; Kim *et al.*, 2013; Kavouras *et al.*, 2015; Tiwari *et al.*, 2015). Mainly formed in burning or pyrolytic processes, PAHs may be emitted from different stationary and mobile sources (Tsai *et al.*, 2001; Chen *et al.*, 2007; Tsai *et al.*, 2012; Kim *et al.*, 2013; Chen *et al.*, 2014; Li *et al.*, 2014; Kavouras *et al.*, 2015; Mwangi *et al.*, 2015; Stogiannidis and Laane, 2015).

Hydrogen-oxygen ($H_2$-$O_2$) proton exchange membrane fuel cells (PEMFCs) are favored as one type of green power generators with the zero-emission claims of pollutants and $CO_2$; however, a $H_2$-$O_2$ PEMFC is another PAHs emission source with little attention (Huang *et al.*, 2015), although PEMFCs are promising alternative power sources for stationary and mobile applications (Wang *et al.*, 2006). The key components of a $H_2$-$O_2$ PEMFC are membrane-electrode assembly (MEA), gas-diffusion layer (GDL), and bipolar/end plate (including carbon/epoxy composite bipolar plates (Huang *et al.*, 2006; Lee and Lee, 2016). The MEA is usually consisted of a PEM (solid electrolyte) and two symmetrical electrodes (anode and cathode) which have precious metal catalysts (e.g., Pt) (Huang *et al.*, 2006; Lai *et al.*, 2012) and non-platinum group metals (Reshetenko, *et al.*, 2016) supported by carbon materials (e.g., carbon black, fiber, and nanotube). Additionally, it is common that the bipolar/end plates and GDLs (e.g., carbon paper (CP) or carbon cloth (CC)) are made using carbon materials (Dicks, 2006; Wissler,

* Corresponding author.
Tel.: +886-8-7703202 ext. 7092; Fax: +886-8-7740256
*E-mail address:* huangkL@mail.npust.edu.tw

2006; Tran *et al.*, 2015; Zeis, 2015). In recent years, research trends of PEMFCs have focused on accelerating the sluggish kinetics of cathode catalyst, minimizing overall Pt content, and increasing membrane proton conductivity (Scofield *et al.*, 2015). However, little attention has been paid to the study of PAH emission from PEMFCs.

In our previous work, we reported the emissions of 21 PAHs from a $H_2$-$O_2$ PEMFC (installed by a lab-prepared MEA with the same Pt loading of 0.5 mg $cm^{-2}$ on anode and cathode) and compared the similarity among the profiles of PAHs of different carbon materials used for fabrication of MEA and GDL (Huang *et al.*, 2015). In this study, we explored the emissions of PAHs from the $H_2$-$O_2$ PEMFC equipped with another lab-made MEA which had the same Pt loading of 0.4 mg $cm^{-2}$ on anode and cathode. The emissions of PAHs were also tested for different commercial MEAs (with different Pt loadings or PEMs) and under different flowrates, temperatures, and sampling periods. The concentration profiles of PAHs emitted from the anode and cathode of PEMFC installed with different MEAs were compared and related to those of carbon materials according to the principle component analysis (PCA). The PAHs-derived $BaP_{eq}$ were also discussed.

## MATERIALS AND METHODS

### *Carbon Materials*

For comparison of PAHs profile similarity, different carbon materials (carbon black, cloth, and paper) were used in the principle component analysis (PCA). Four brands of carbon blacks or graphite powders tested in this work were (Vulcan) XC-72/XC-72R (Cabot, supplied from E-TEK), Alfa (acetylene carbon black, Alfa Aesar), and Black Pearls (BP) 2000 (Cabot). Furthermore, the other carbon materials were two types of carbon cloth with/without water-proof treatment (denoted as WPCC and CC, respectively) and one type of water-proofed carbon paper (WPCP) from Toray. The characteristics of these seven carbon materials were reported in our earlier work (Huang *et al.*, 2015).

### *Membrane-Electrode Assembly (MEA), Fuel Cell Emission Test, and PAH Sampling*

The heart of a PEMFC is membrane-electrode assembly (MEA) which is usually consisted of a proton exchange membrane (solid electrolyte), two dispersed catalyst layers, and two gas diffusion layers (GDL) (Fig. 1). The lab-made MEA (denoted as E-TEK2) tested in this study was made by hot pressing/sandwiching a Nafion-117 (Dupont) with a GDL-supported anode (E-TEK), and a GDL-supported cathode (E-TEK). Three commercial MEAs (E-TEK, SGL, and GORE) were also tested and compared in this study. Table 1 provides the anode Pt loadings, cathode Pt loadings, and proton exchange membranes of all the five tested MEAs.

The single $H_2$-$O_2$ PEMFC used in PAH emission tests had an MEA symmetrically sandwiched by Telfon gaskets, carbon (graphite) blocks (with gas flow channel), and copper current collectors (Fig. 1). The single cell was installed on a standard fuel cell test station that worked at 65°C (80°C and 70°C for the anode and cathode humidifiers, respectively) and 0.6 V for 12–36 h for PAH collection. Two mass flow controllers were used to control the anode hydrogen and cathode oxygen flow rates of 52 and 35 sccm, respectively, corresponding to 1.5 and 2 times of the stoichiometric requirements for the anode and cathode feeding gases, respectively (Huang *et al.*, 2006; Huang *et al.*, 2015). The details of sampling system connected to the single cell and PAH collection were provided in our previous work (Huang *et al.*, 2015). The anode and cathode sampling volumes for PAH collection were the same (57.6 L) at various anode/cathode flowrates of 52/35, 25/25, 100/100, and 200/200 sccm, while at the anode/cathode flowrates of 52/35 sccm the anode/cathode sampling volumes for 12, 24, and 36 h sampling were 37.4/25.2, 74.9/50.4, and 112/75.6 L, respectively). The PAH collection was triplicate (n = 3) for each experiment.

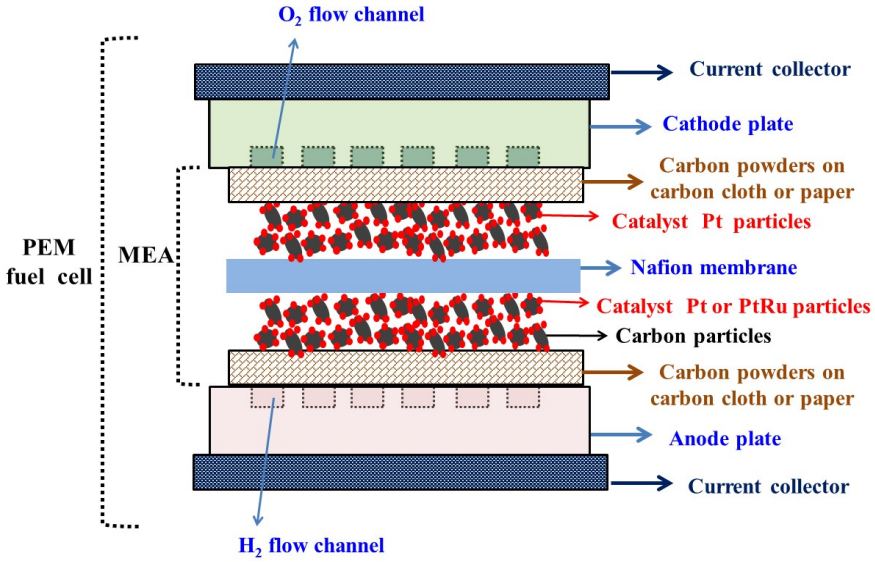


**Fig. 1.** The scheme of single PEMFC installed with an MEA for PAH emission experiments.

**Table 1.** Total-PAHs (μg $Nm^{-3}$), Total-$BaP_{eq}$ (μg $Nm^{-3}$), and emission factors (EFs) (μg $g^{-1}$-MEA) in anode/cathode gas emissions of the single PEMFC installed with different membrane electrode assemblies (MEAs) having different anode Pt loadings (APL) (mg $cm^{-2}$), cathode Pt loadings (CPL) (mg $cm^{-2}$), and Nafion (N) membranes.

| | | Lab-made | Commercial | | |
|---|---|---|---|---|---|
| MEA | | E-TEK2 | E-TEK | SGL | GORE |
| APL | | 0.40 | 0.30 | 0.30 | 0.60[#] |
| CPL | | 0.40 | 0.30 | 0.30 | 0.45 |
| Membrane | | N117 | N211 | N117 | N117[$] |
| Total-PAHs | anode | 9.75 ± 0.60 | 9.54 ± 0.28 | 9.22 ± 0.36 | 10.1 ± 1.05 |
| | cathode | 11.7 ± 1.13 | 11.1 ± 0.89 | 11.0 ± 0.75 | 11.8 ± 1.13 |
| | sum[*] | 21.4 ± 1.28 | 20.7 ± 0.93 | 20.2 ± 0.83 | 21.9 ± 1.54 |
| Total-$BaP_{eq}$ | anode | 0.25 ± 0.02 | 0.24 ± 0.01 | 0.23 ± 0.01 | 0.26 ± 0.04 |
| | cathode | 0.43 ± 0.06 | 0.41 ± 0.06 | 0.40 ± 0.05 | 0.44 ± 0.08 |
| | sum[*] | 0.68 ± 0.07 | 0.65 ± 0.06 | 0.63 ± 0.06 | 0.70 ± 0.09 |
| PAH EF | sum[*] | 7.91 ± 0.47 | 11.5 ± 0.21 | 13.3 ± 0.55 | 3.17 ± 0.22 |

#: PtRu

$: modified N117 membrane.

*: sum of anode and cathode gas PAH emissions.

### *PAH Analysis and Quality Control*

In this study, we measured 21 PAHs: Naphthalene (Nap), Acenaphthylene (AcPy), Acenaphthene (Acp), Fluorene (Flu), Phenanthrene (PA), Anthracene (Ant), Fluoranthene (FL), Pyrene (Pyr), Benzo(a)anthracene (BaA), Chrysene (CHR), Cyclopenta(c,d)pyrene (CYC), Benzo(b)fluoranthene (BbF), Benzo(k)fluoranthene (BkF), Benzo(e)pyrene (BeP), Benzo(a)pyrene (BaP), Perylene (PER), Indeno(1,2,3,-cd)pyrene (IND), Dibenzo(a,h)anthrance (DBA), Benzo(b)chrycene (BbC), Benzo(ghi)perylene (BghiP) and Coronene (COR).

For PAHs extraction and analysis, each carbon material sample was weighed on an electronic five-digit scale (AND GR-120) and placed into a pre-cleaned thimble that was then extracted in a Soxhlet extraction apparatus. All carbon materials, cell emission gas, and cell effluent samples were extracted in the Soxhlet extraction apparatus for 24 hours with 1:1 (v/v) n-hexane/dichloromethane. The extracts were then concentrated, cleaned via a silica column, and reconcentrated by purging with ultra-pure nitrogen to 1.0 or 0.5 mL prior to analysis. The identification and quantification of PAHs was performed via gas chromatograph/mass spectrometer (GC/MS) measurements using a GC (Hewlett-Packard 5890A) with a Hewlett-Packard capillary column (HP Ultra 2- 50 m × 0.32 mm i.d., 0.17 μm film thickness), and a mass selective detector (MSD) (Hewlett-Packard 5972). The operating conditions of GC/MS were stated elsewhere (Huang *et al.*, 2015). The response factors of the PAH standard solution were used to calculate the masses of the sampled PAHs at the same GC/MS relative retention time (RRT).

The total-PAHs concentration was obtained from the sum of the concentrations of 21 PAH species for each collected sample. To assess the PAH homologue distribution of each sample, the 21 PAH species were classified into three catagories: low molecular weight (LMW-PAHs, 2-/3-ring PAHs: NaP, AcPy, AcP, Flu, Ant, and PA), middle molecular weight (MMW-PAHs, 4-ring PAHs: FL, Pyr, BaA, and CHR), and high molecular weight (HMW-PAHs, 5-/6-/7-ring PAHs: CYC, BbF, BkF, BeP, BaP, PER, DBA, BbC, IND, BghiP, and COR).

All PAHs were corrected with procedural blanks that were consistently analyzed with the samples. The PAHs were quantified based on the retention times and areas under the peaks obtained from the calibration standards. At least five standard concentrations, covering the concentrations of interest, were used in PAH analysis calibration. The correlation coefficients of the calibration curves were 0.995–0.998.

The quality assurance (QA) and quality control (QC) procedures for PAHs GC/MS analysis were reported in our previous work (Huang *et al.*, 2015). Ten consecutive injections of a PAH 610-M standard yielded an average relative standard deviation (RSD) of the GC/MS integration area of 3.0% with a range of 0.8–5.1%. The total recovery efficiencies of PAHs from seven consecutive injections ranged from 87 to 104%, while the average recoveries of the five internal standards were 85–93% across seven consecutive injections.

The coefficients of variation for repeat injections of the standard solution (containing PAH Mixture-610 M (16 PAHs) and five Merck PAH standards) were all less than 5% for all of the analyzed PAHs, whereas those obtained by replicate analysis were 2–10%. Analyses of serial dilutions of PAH standards revealed the limits of detection (LODs) of GC/MS to be between 0.071 and 0.936 ng for the 21 PAH compounds. The limit of quantification (LOQ) was defined as the LOD divided by the sampling volume. The LOQ values of the 21 PAH compounds for carbon material and cell emission gas were 0.008–0.016 ng $g^{-1}$ and 0.076–0.175 ng $Nm^{-3}$, respectively.

## RESULTS AND DISCUSSION

### *Effect of Flowrate on PEMFC PAHs and PAHs-associated $BaP_{eq}$ Emission*

Fig. 2 shows the anode and cathode concentration profiles of PAHs emitted from the single fuel cell installed with the E-TEK2 (lab-made) MEA operated at 65°C and

different flowrates. The cell was first tested at the anode hydrogen and cathode oxygen flow rates of 52 (18.46 h) and 35 (27.43 h) sccm, respectively, corresponding to 1.5 and 2 times of the stoichiometric requirements for the anode and cathode feeding gases, respectively (Huang *et al.*, 2006; Huang *et al.*, 2015). For comparison, the flowrates of anode/cathode of 25/25, 100/100, and 200/200 sccm were also tested, while their sampling volumes were the same as that of 52/35 sccm. At anode/cathode flowrates of 52/35 sccm, the concentrations of PAHs in anode emission

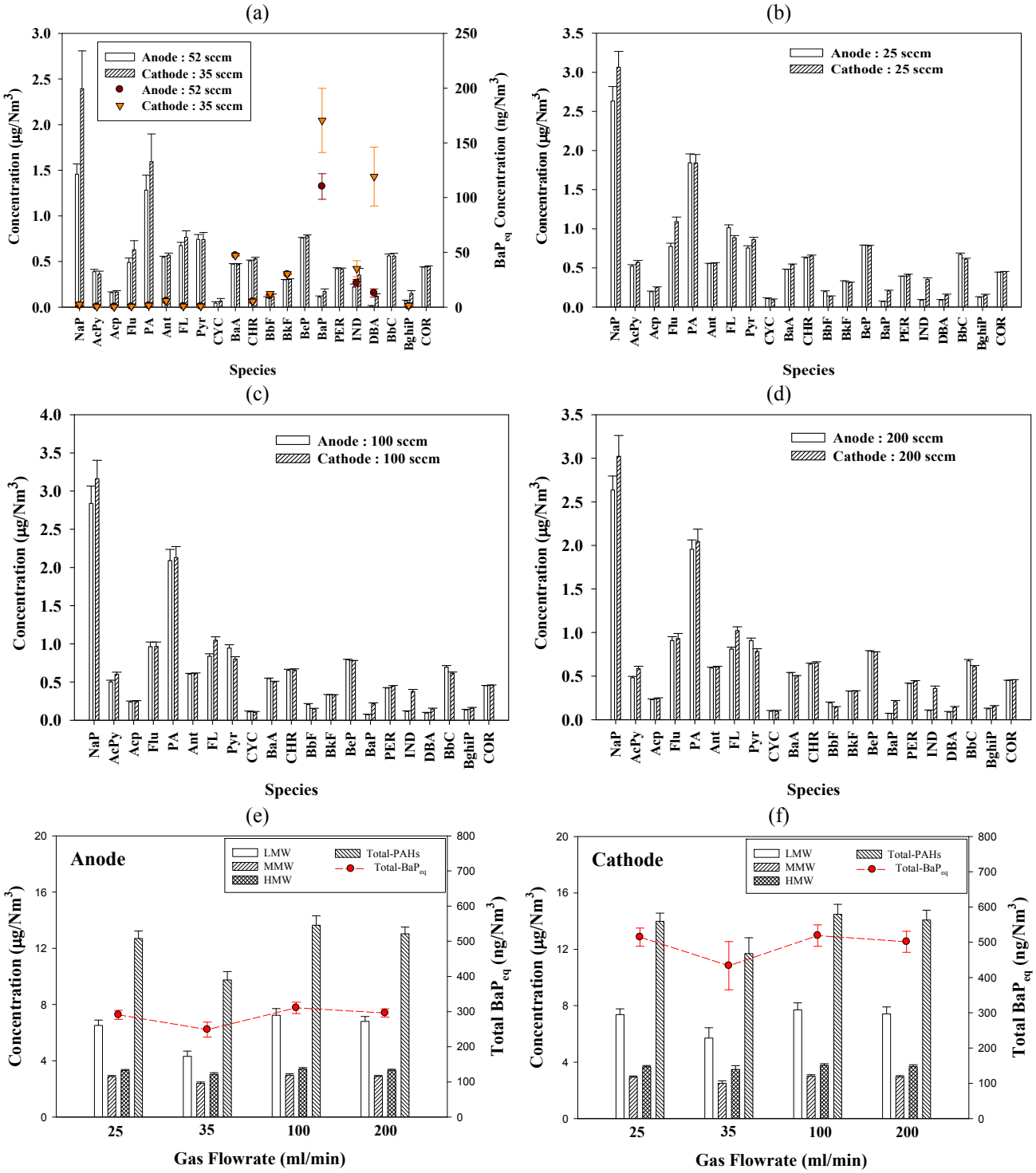


**Fig. 2.** Characteristic profiles of emitted PAHs at different PEMFC flowrates (65°C): (a) anode/cathode = 52/35 mL $min^{-1}$, (b) anode/cathode = 25/25 mL $min^{-1}$, (c) anode/cathode = 100/100 mL $min^{-1}$, (d) anode/cathode = 200/200 mL $min^{-1}$; concentrations of corresponding LMW-, MMW-, HMW-, and Total-PAHs and Total-$BaP_{eq}$ at (e) anode and (f) cathode (n = 3) (E-TEK2).

gas ranged from 0.013 ± 0.004 (DBA) to 1.45 ± 0.11 (Nap) μg $Nm^{-3}$; for cathode emission gas, the corresponding data were 0.066 ± 0.028 (CYC) to 2.39 ± 0.42 (Nap) μg $Nm^{-3}$ (Fig. 2(a)). Among the 21-PAH species, Nap was the most dominant one, followed by PA, BeP, FL, Pyr, BbC, Ant, or Flu in both anode and cathode gas emissions; however, the concentration was higher in the cathode gas emission than in the anode gas emission for the same PAH species, although both anode and cathode gas emissions had similar concentration profiles of PAHs. This phenomenon was also observed when the anode and cathode used the same flowrate (anode/cathode flowrate = 25/25, 100/100, or 200/200 sccm (Figs. 2(b), 2(c), and 2(d), respectively)).

To have the same gas sampling volume, the sampling time on the anode side was shorter than on the cathode side, since the flowrate was greater for the former than for the latter. Furthermore, the two electrodes were operated at different potentials (anode: < 1.23 V (theoretical) vs. standard hydrogen electrode (SHE); cathode: ~0 V vs. SHE) with different electrochemical reactions (anodic hydrogen oxidation ($H_2 \rightarrow 2H^+ + 2e^-$) and cathodic oxygen reduction ($2H^+ + 2e^- + 1/2O_2 \rightarrow H_2O$), respectively). More water should be present on the cathode side than on the anode side because of the product (water) generated from the oxygen reduction reaction. In the anode and cathode gas emissions at anode/cathode flowrate = 52/35 sccm, the concentrations of Total-PAHs were 9.75 ± 0.60 and 11.7 ± 1.13 μg $Nm^{-3}$, respectively (Figs. 2(e) and 2(f), respectively). Both the anode and cathode gas emissions exhibited different concentrations of molecular-weight (MW) classified PAHs with the following order: LMM- > HMM- > MMM-PAHs (anode: 4.32 ± 0.37, 3.03 ± 0.13, and 2.39 ± 0.10 μg $Nm^{-3}$, respectively; cathode: 5.71 ± 0.73, 3.48 ± 0.27, and 2.51 ± 0.17 μg $Nm^{-3}$, respectively); this phenomenon did not change at anode/cathode flowrate = 25/25, 100/100, and 200/200 sccm.

When the PEMFC was operated at anode/cathode flowrate = 25/25, 100/100, and 200/200 sccm, their anode or gas emissions showed similar Total-PAHs concentrations, but these values were greater than that at 52/35 sccm. This result is attributable to the more concentration variation for LMW-PAHs than for MMW- and HMW-PAHs (particularly Nap) during the operation of PEMFC at different anode/cathode flowrates. Therefore, the emission of LMW-PAHs was more influenced by flowrate than by the different electrochemical reactions of anode and cathode; additionally, the emission of Nap was more influenced by flowrate than those of the other PAH species. The PAHs in the anode or cathode emission gas should be associated with the desorption of the PAHs adsorbed on the carbon materials of PEMFC during operation, although the graphitic structure of carbon materials might have strong interactions with PAHs through π-π interactions (Kah *et al.*, 2011) and PAHs are relatively easier to adsorb on than to desorb from the surface of carbon blacks (Moninot, 2010).

In addition to concentration, compound structure also influences the carcinogenic potency of each PAH. PAH compounds with more rings (e.g., BaP, DBA, BaA, BbF, BkF, and IND) are usually more toxic. The benzo(a)pyrene (BaP)-equivalent carcinogenic potency ($BaP_{eq}$) of a PAH species can be calculated by the product of its toxic equivalence factor (TEF) and concentration (Nisbet and LaGoy, 1992). Of all the 21-PAH, BaP and DBA had the highest and second highest $BaP_{eq}$ concentrations in cathode emission gas, and BaP also exhibited the highest $BaP_{eq}$ concentration in anode emission gas because of the highest TEF values of these two compounds. The PAH-derived Total-$BaP_{eq}$ values of different flowrates were in the order 25/25 (0.29 ± 0.01/0.51 ± 0.03 μg $Nm^{-3}$) ≈ 100/100 (0.31 ± 0.02/0.52 ± 0.03 μg $Nm^{-3}$) ≈ 200/200 (0.30 ± 0.01/0.50 ± 0.03 μg $Nm^{-3}$) > 52/35 (0.25 ± 0.02/0.43 ± 0.06 μg $Nm^{-3}$) sccm.

### *Effect of Sampling Time on PEMFC PAHs and PAHs-associated $BaP_{eq}$ Emission*

The sampling of PAHs emission was performed at the same flowrate (anode = 52 and cathode = 35 sccm) but different sampling periods (12, 24, and 36 h) for the PEMFC installed with the E-TEK2 (lab-made) MEA to examine if the concentration profile and amount of PAHs emission change. Approximately, the concentration profiles of emitted PAHs collected within the sampling periods of 12, 24, and 36 h were similar (Figs. 3(a) and 3(b), and (c), respectively)). Among the 21-PAH, Nap had the highest concentration in anode emission gas, while DBA and CYC exhibited the lowest concentrations in anode and cathode emission gases, respectively. In both anode and cathode emission gases, the concentrations of MW-classified PAHs were in the order LMW- (anode = 5.44 ± 0.60−3.44 ± 0.44 and cathode = 7.33 ± 0.06−4.95 ± 0.81 μg $Nm^{-3}$) > HMW- (anode = 4.35 ± 0.15−1.88 ± 0.08 and cathode = 6.38 ± 0.20−2.78 ± 0.29 μg $Nm^{-3}$) > MMW-PAHs (anode = 3.44 ± 0.12−1.48 ± 0.07 and cathode = 4.75 ± 0.13−1.99 ± 0.18 μg $Nm^{-3}$) (Figs. 3(d), and 3(e)).

Again, the concentration of LMW-, MMW-, HMW-, or Total-PAHs was smaller in anode emission gas than in cathode emission gas. Moreover, the concentrations of LMW-, MMW- and HMW-PAHs decreased with an increasing sampling time; consequently, the concentrations of Total-PAHs sum (anode + cathode = 31.7 ± 0.68, 20.4 ± 1.03 and 16.5 ± 0.99 μg $Nm^{-3}$ for 12, 24, and 36 h, respectively) and Total-$BaP_{eq}$ sum (anode + cathode = 0.93 ± 0.06, 0.68 ± 0.08 and 0.54 ± 0.07 μg $Nm^{-3}$ for 12, 24, and 36 h, respectively) decreased as the increase of sampling time. Nevertheless, the mass or amount of Total-PAHs in anode or cathode emission gas followed the order 36 > 24 > 12 h. In this study, the masses of anode and cathode Total-PAHs collected for sampling n hours are denoted as $MA_{nh}$ and $MC_{nh}$, respectively, and the sum of $MA_{nh}$ and $MC_{nh}$ is represented by $MS_{nh}$. It was found that the $MA_{12h}/MA_{36h}$ and $MA_{24h}/MA_{36h}$ were 0.65 and 0.80, respectively, and the $MC_{12h}/MC_{36h}$ and $MC_{24h}/MC_{36h}$ were 0.63 and 0.84, respectively. Accordingly, the $MS_{12h}$ and $MS_{24h}$ accounted for 64% and 82% of $MS_{36h}$, respectively. It is concluded that around 80% of PAHs were blown out via the anode and cathode emission gases of PEMFC at anode/cathode = 52/35 sccm (65°C), and the Total-PAHs emission rate (mass per hour) decreased with an increasing time.

### *Effect of Temperature on PEMFC PAHs and PAHs-associated $BaP_{eq}$ Emission*

Fig. 4(a) shows the concentration profiles of 21-PAH in anode and cathode emission gases at PEMFC (using the E-TEK2 (lab-made) MEA) temperature = 90°C at anode/cathode = 52/35 sccm. The concentration profiles of 21-PAH in anode and cathode emission gases at 90°C were similar to those at 65°C. Furthermore, the orders of

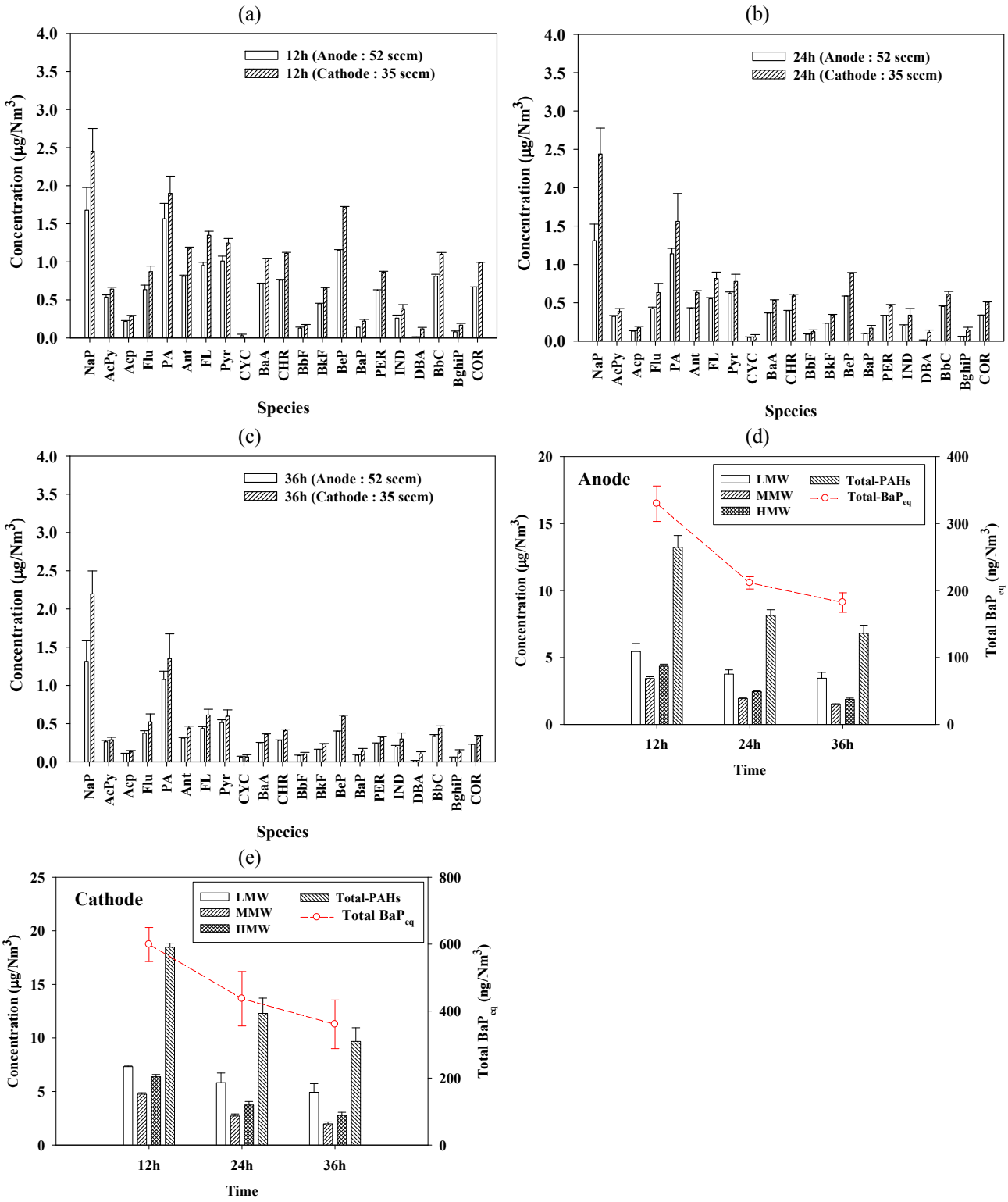


**Fig. 3.** Characteristic profiles of PEMFC emitted PAHs collected at different sampling times (65°C): (a) 12 h, (b) 24 h, and (c) 36 h; concentrations of corresponding LMW-, MMW-, HMW-, and Total-PAHs and Total-$BaP_{eq}$ at (d) anode and (e) cathode (n = 3) (E-TEK2).

magnitude of LMM-, MMM-, HMM-, and Total-PAHs concentrations were also similar at both temperatures (Fig. 4(b)). However, the concentrations of LMW-, MMW-, and HMW-PAHs were slightly higher at 90°C than at 65°C, possibly because the rise of PEMFC operating temperature enhanced the desorption of PAHs. At 90°C, the concentrations of anode LMW-, MMW-, HMW-, and Total-PAHs were 5.11 ± 0.40, 2.44 ± 0.05, 3.20 ± 0.07, and 10.8 ± 0.49 μg $Nm^{-3}$, respectively, while the cathode ones were 6.30 ± 0.66, 2.58 ± 0.11 3.64 ± 0.18, and 12.5 ± 0.95 μg $Nm^{-3}$, respectively. As a result, the sum of anode and cathode Total-PAHs emission concentrations was slightly higher at 90°C (23.3 ± 1.07 μg $Nm^{-3}$) than at 65°C (21.4 ± 1.28 μg $Nm^{-3}$). The sum of anode and cathode Total-$BaP_{eq}$ was 0.30 ± 0.04 μg $Nm^{-3}$ at 90°C.

### *Effect of MEA on PEMFC PAHs and PAHs-associated $BaP_{eq}$ Emission*

Three commercial MEAs (E-TEK, SGL, and GORE) were tested and compared to the lab-made E-TEK2 MEA for the PEMFC PAHs emission. The anode and cathode Pt loadings of E-TEK2 MEA are the same (0.40 mg $cm^{-2}$) (Table 1). This was also true for the E-TEK and SGL MEAs (0.30 mg $cm^{-2}$). However, for GORE MEA, the anode and cathode catalysts were PtRu (0.60 mg $cm^{-2}$) and Pt (0.45 mg $cm^{-2}$), respectively. The E-TEK2 and SGL MEAs used the same proton exchange membranes (PEMs) (Nafion (N) 117), while the PEMs of E-TEK and GORE MEAs were N211 and modified-N117 (composite), respectively. The thicknesses of these PEMs was in the order N211 < N117 < modified-N117.

The concentration profiles of PAHs in anode and cathode emission gases for using E-TEK was similar to those for using E-TEK2 as the MEA of PEMFC, although the former had lower anode/cathode Pt loadings than the latter (Fig. 5(a)). Likewise, similar concentration profiles of PAHs were also observed when using SGL or GORE as the MEA of PEMFC (Figs. 5(b) and 5(c)). Moreover, the concentrations of PAHs in anode and cathode emission gases of LMW- (anode = 3.96 ± 0.22–4.54 ± 0.68 and cathode = 5.22 ± 0.43–5.80 ± 0.65 μg $Nm^{-3}$), MMW- (anode = 2.32 ± 0.06–2.44 ± 0.16 and cathode = 2.42 ± 0.14–2.52 ± 0.19 μg $Nm^{-3}$), or HMW-PAHs (anode = 2.94 ± 0.08–3.09 ± 0.21 and cathode = 3.34 ± 0.22–3.51 ± 0.31 μg $Nm^{-3}$) for these four cases followed the order GORE > E-TEK2 > E-TEK > SGL (Figs. 5(d) and 5(e)). Therefore, the same order was obeyed in Total-PAHs concentration: GORE > E-TEK2 > E-TEK > SGL (with the ranges of anode, cathode, and sum Total-PAHs = 10.1 ± 1.05–9.22 ± 0.36, 11.8 ± 1.13–11.0 ± 0.75, and 21.9 ± 1.54–20.2 ± 0.83 μg $Nm^{-3}$, respectively); likewise, the concentrations of Total-$BaP_{eq}$ were in the order GORE > E-TEK2 > E-TEK > SGL (with the ranges of anode, cathode, and sum Total-$BaP_{eq}$ = 0.26 ± 0.04–0.23 ± 0.01, 0.44 ± 0.08–0.40 ± 0.05, and 0.70 ± 0.09–0.63 ± 0.06 μg $Nm^{-3}$, respectively) (Table 1). Nevertheless, the PAHs emission factors (sum of anode and cathode) of the single PEMFC equipped with these MEAs varied with the order SGL > E-TEK > E-TEK2 > GORE (13.3 ± 0.55, 11.5 ± 0.21, 7.91 ± 0.47, and 3.17 ± 0.22 μg $g^{-1}$-MEA, respectively) although these data were obtained at the same cell voltage (0.6 V) with different power densities of 490, 715, 655, and 1045 mW $cm^{-2}$, respectively. This result is attributed to the significant difference in MEA weight (catalyst, carbon support, PEM, and GDL), because the difference in sum (anode plus cathode) of Total-PAHs for these four cases was small (21.9 ± 1.54–20.2 ± 0.83 μg $Nm^{-3}$). As mentioned, the PAHs collected in the PEMFC exhaust were from the desorption of those originally absorbed on PEMFC carbon materials during operation; moreover, the PAH emission rate decreased with an increasing sampling time. Therefore, it is reasonable to infer that most of the desorbable PAHs might be blown out from the PEMFC around tens of hours.

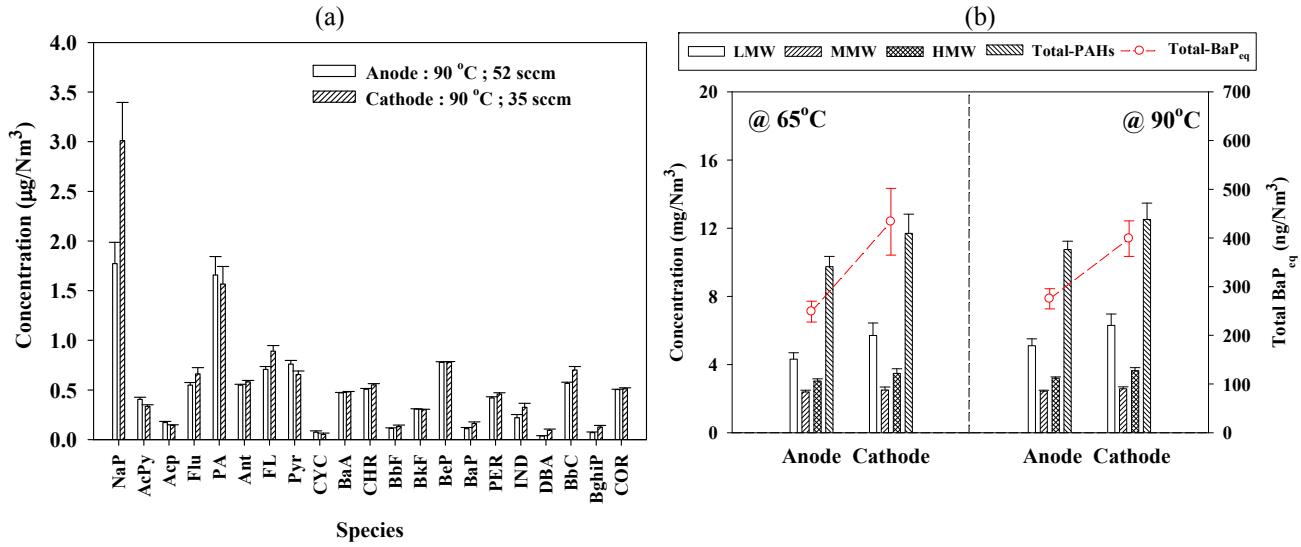


**Fig. 4.** Characteristic profiles of emitted PAHs at 90°C (a) and concentrations of corresponding LMW-, MMW-, HMW-, and Total-PAHs and Total-$BaP_{eq}$ at different temperatures (anode = 52 mL $min^{-1}$, cathode = 35 mL $min^{-1}$) (n = 3) (b) (E-TEK2).

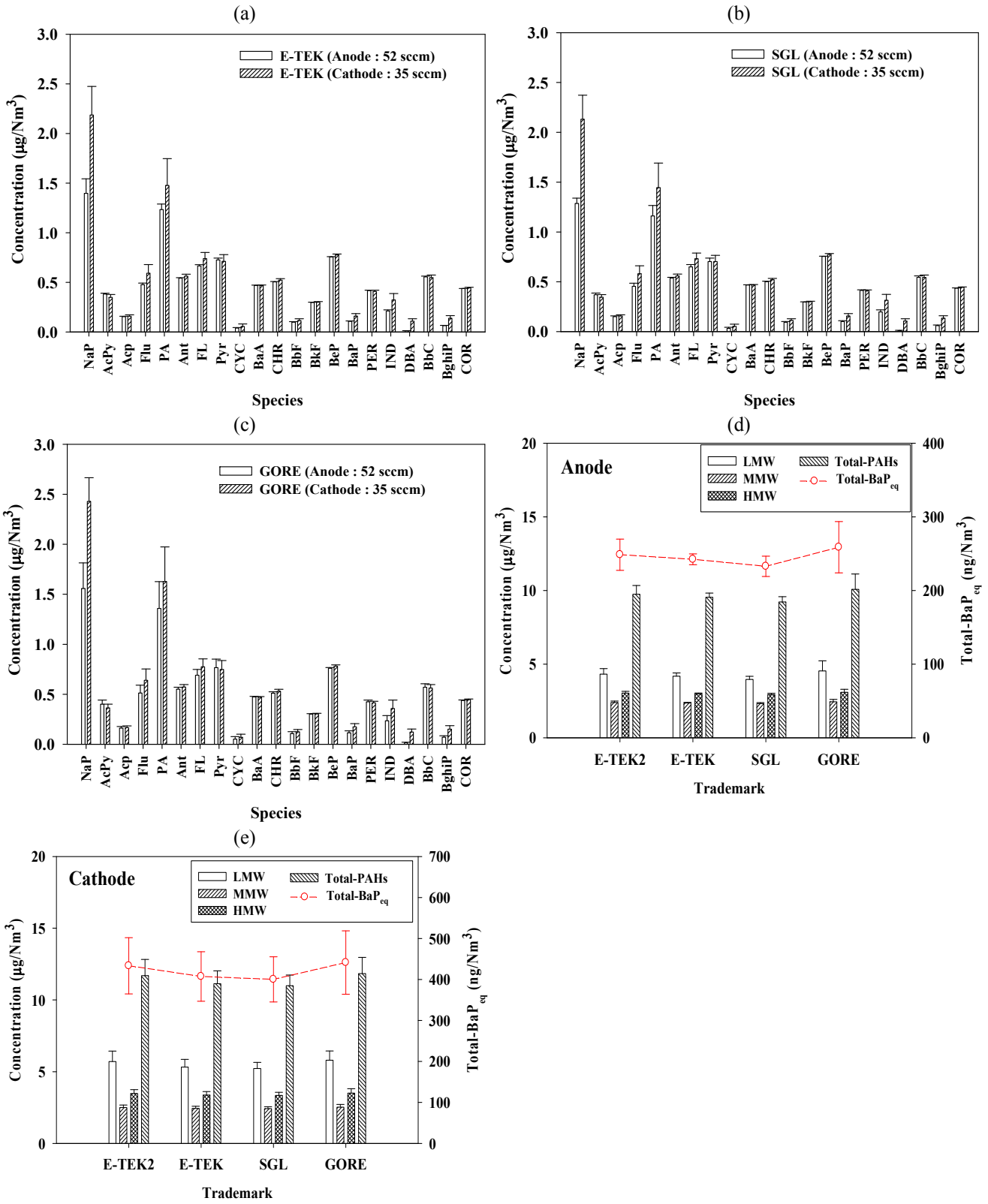


**Fig. 5.** Characteristic profiles of PAHs emitted from the PEMFC using different commercial MEAs: (a) SGL, (b) E-TEK, and (c) GORE; concentrations of LMW-, MMW-, HMW-, and Total-PAHs and Total-$BaP_{eq}$: (d) anode and (e) cathode (n = 3).

Accordingly, it is inappropriate to directly compare the PAH emission factors obtained in this study with those of fuel consumption or driving distance (mileage) based data reported in the literature.

Fig. 6 shows the polarization (current-potential) curves for the PEMFC installed with commercial MEAs, indicating

that the performances of these MEAs were in the order SGL < E-TEK < GORE, chiefly because the anode/cathode catalyst loadings were greater for GORE than for SGL and E-TEK, and the PEM of E-TEK was thinner than that SGL to lower the ohmic resistance (Table 1). The potential drop in ohmic region was slightly greater for E-TEK2 than for E-TEK because the former had a thicker PEM than the latter, despite the opposite trend of their Pt loadings. At current density greater than 1000 mA $cm^{-2}$, the cell voltage of PEMFC using SGL steeply dropped, primarily because of the significant concentration polarization (loss due to mass transport) associated with cathode flooding (Huang *et al.*, 2006; Scofield *et al.*, 2015).

***Comparison of PAHs Concentration Profiles (MEAs vs. Carbon Materials)***

As mentioned, the PAHs in the anode or cathode emission gas should be related to the desorption of carbon material bound PAHs during the operation of the PEMFC. In this study, therefore, the principle component analysis (PCA) was performed to compare the concentration profiles of PAHs in anode and cathode emission gases of PEMFC equipped with the lab-made and commercial MEAs with the content profiles of PAHs of carbon materials. Fig. 7(a) displays two groups for the comparison of PAH profiles for carbon materials vs. (lab-made) E-TEK2 MEA in the PCA (SPSS 22). One of these two groups with a triangle symbol had members of WPCC, XC-72R, and Alfa, while the other group with a circle symbol was consisted of XC-72, WPCP, CC, BP2000, E-TEK2_C, and E-TEK2_A. Accordingly, the PAH profiles of anode (A) and cathode (C) emission gases when using E-TEK2 as the MEA of PEMFC (E-TEK2_A, and E-TEK2_C) were similar, and these PAH profiles were also similar to those of two carbon blacks (XC-72 and BP2000) and two GDL materials (water-proof carbon paper (WPCC) and carbon cloth (CC)), because the same group members exhibit similarity in PCA based on Bartlett's sphericity test ($p < 0.05$) and the KMO (Kaiser-Mayer-Olkin) index. Moreover, it is common to use Vulcan XC-72 and XC-72R in E-TEK MEAs (Dicks, 2006; Lavall *et al.*, 2008; Hwang *et al.*, 2009). Therefore, the result of PCA supports the relation of PAHs absorbed on carbon materials with those emitted from the anode and cathode gases of PEMFC.

Dissimilarly, when the cases of three commercial MEAs were included in the PAH profile comparison in PCA, the type of grouping changed; all the carbon materials were in the same group, while the MEAs were in the other group (Fig. 7(b)). This phenomenon can be explained by the much more similarity in PAH profile for the lab-made MEA (E-TEK2) vs. commercial ones (SGL, E-TEK, and GORE) than for the E-TEK2 vs. carbon materials.

In PCA, the Factors 1 and 2 together accounted for 89.3% and 92.5% of the total variance in Figs. 7(a) and 7(b), respectively. The Factor 1, much more dominant than Factor 2, was probably associated with the fabrication method of carbon materials. In this study, the PAHs of tested carbon materials should be chiefly in relation to pyrogenic manufacturing, since these materials are often manufactured in factories, although PAHs can be generated from pyrogenic, petrogenic, or biogenic/diagenetic sources (Stogiannidis and Laane, 2015). On the other hand, the Factor 2 was likely associated with property of carbon material, because different raw materials are used for carbon black production in different companies (Huang *et al.*, 2015), which may cause the difference in PAH adsorption on carbon materials. Accordingly, attention should be paid to PEMFC carbon materials for their relation to PEMFC PAHs emission.

## CONCLUSIONS

In this study, at anode/cathode gas flowrates of 52/35 sccm and using the lab-made E-TEK2 as the MEA of PEMFC, the concentrations of PAHs in anode and cathode emission gases ranged from 0.013 ± 0.004 (DBA) to 1.45 ± 0.11 (Nap) and 0.066 ± 0.028 (CYC) to 2.39 ± 0.42 (Nap) μg $Nm^{-3}$, respectively. Among the 21-PAH species, Nap was the most dominant one, followed by PA, BeP, FL, Pyr,

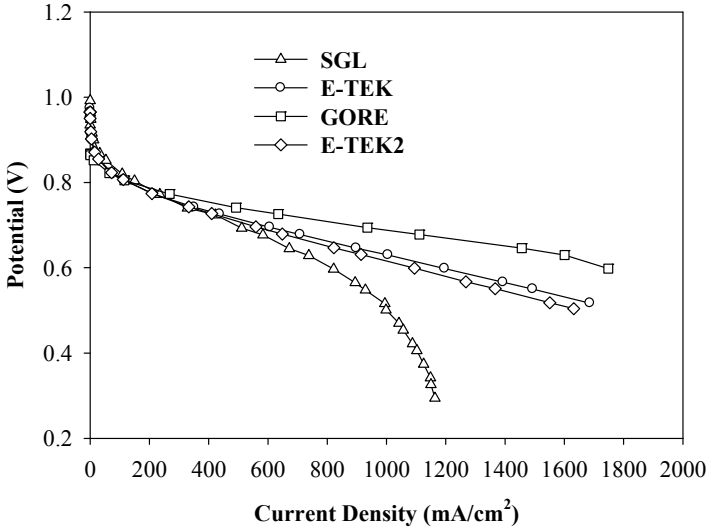


**Fig. 6.** Polarization (current-potential) curves for the PEMFC installed with different MEAs.

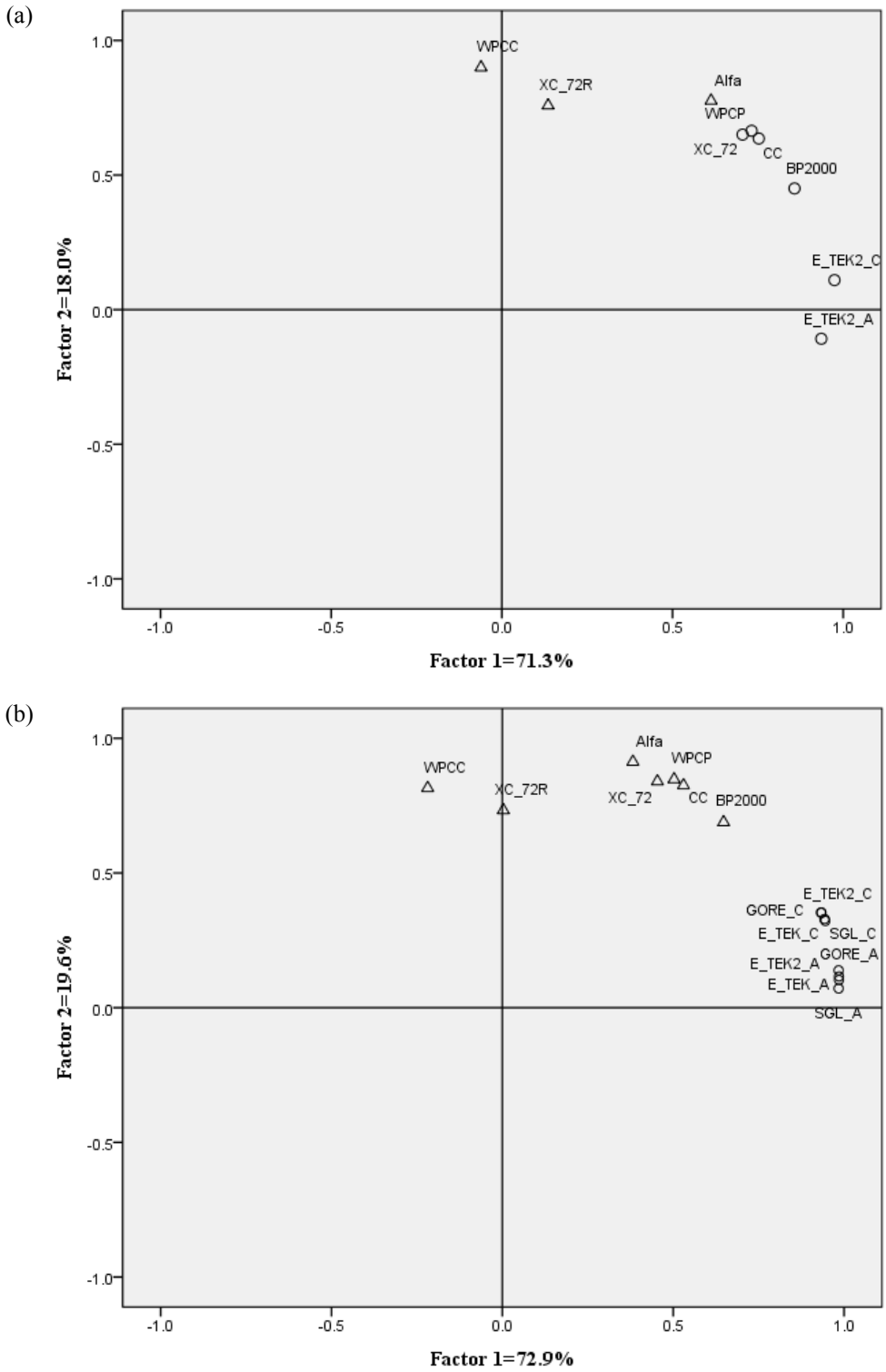


**Fig. 7.** Principle Component Analysis (PCA) for the PAHs of anode/cathode emission gases of PEMFC installed with different MEAs and the PAHs of carbon materials (carbon black: XC-72, XC-72R, Alfa, and BP2000; carbon cloth (CC), water-proof CC (WPCC), and WP carbon paper (WPCP)).

BbC, Ant, or Flu in both anode and cathode gas emissions. The concentrations of molecular-weight classified PAHs were in the order LMW- > HMW- > MMW-PAHs. The concentrations of Total-PAHs and Total-$BaP_{eq}$ was higher in the cathode gas emission (11.7 ± 1.13 and 0.43 ± 0.06 μg $Nm^{-3}$, respectively) than in the anode one (9.75 ± 0.60 and 0.25 ± 0.02 μg $Nm^{-3}$, respectively).

When the anode/cathode gas flowrates were greater or smaller than 52/35 sccm at the same sampling volume, the emission concentrations of Total-PAHs and Total-$BaP_{eq}$

increased, although their PAHs concentration profile were similar to that at 52/35 sccm. The concentrations of LMW-, MMW-, HMW-, and Total-PAHs decreased with an increasing sampling time, but an opposite trend was observed for the mass of Total-PAHs. About 64% and 82% of PAH mass were emitted within 12 and 24 h, respectively, based on 36 h sampling. At anode/cathode gas flowrates = 52/35 sccm, the sum of anode and cathode Total-PAHs or Total-$BaP_{eq}$ emission concentrations was slightly higher at 90°C than at 65°C using E-TEK2 MEA. For the PEMFC using different MEAs, the sums of anode and cathode Total-PAHs or Total-$BaP_{eq}$ emission concentrations were in the order GORE > E-TEK2 > E-TEK > SGL (21.9 ± 1.54, 21.4 ± 1.28, 20.7 ± 0.93, and 20.2 ± 0.83μg $Nm^{-3}$, respectively), while the corresponding sums of anode and cathode PAHs emission factors varied with the order SGL > E-TEK > E-TEK2 > GORE (13.3 ± 0.55, 11.5 ± 0.21, 7.91 ± 0.47, and 3.17 ± 0.22 μg $g^{-1}$-MEA, respectively). The performances of commercial MEAs were in the order SGL < E-TEK ≈ E-TEK2 < GORE.

The PAH profiles of anode and cathode emission gases when using E-TEK2 as the MEA of PEMFC were similar to those of some carbon materials, although the anode and cathode emission PAH profiles for using E-TEK2 were more similar to those for using the commercial MEAs. It is concluded that the PAHs can be emitted from the $H_2$-$O_2$ PEMFC, so it is not a zero-emission power generator. It is necessary to regulate the levels of PAHs on PEMFC carbon materials.

## ACKNOWLEDGEMENT

The authors would like to thank the Ministry of Science and Technology, Taiwan, R.O.C. for financially supporting this research under Grant No. NSC 96-2211-E-020-011-MY2.

## REFERENCES

Chen, S.J., Su, H.B., Chang, J.E., Lee, W.J., Huang, K.L., Hsieh, L.T., Huang, Y.C., Lin, W.Y. and Lin, C.C. (2007). Emissions of polycyclic aromatic hydrocarbons (PAHs) from the pyrolysis of scrap tires. *Atmos. Environ.* 41: 1209–1220.

Chen, W.H., Han, J., Qin, L.B. Furuuchi, M. and Mitsuhiko, H. (2014). The emission characteristics of PAHs during coal and sewage sludge co-combustion in a drop tube furnace. *Aerosol Air Qual. Res.* 14: 1160–1167.

Dicks, A.L. (2006). The role of carbon in fuel cells. *J. Power Sources* 156: 128–141.

Huang, K.L., Lai, Y.C. and Tsai, C.H. (2006). Effects of sputtering parameters on the performance of electrodes fabricated for proton exchange membrane fuel cells. *J. Power Sources* 156: 224–231.

Huang, K.L., Tsai, T.H., Tsai, J.H., Chen, S.J., and Lee, W.J. (2015). Emission of PAHs from a single hydrogen-oxygen PEM fuel cell: In relation to fuel cell carbon materials. *Aerosol Air Qual. Res.* 15: 2654–2667.

Hwang, J.Y., Chatterjee, A., Shen, C.H., Wang, J.H., Sun, C.L., Chyan, O., Chen, C.W., Chen, K.H. and Chen, L.C. (2009). Mesoporous active carbon dispersed with ultra-fine platinum nanoparticles and their electrochemical properties. *Diamond Relat. Mater.* 18:303–306.

Kah, M., Zhang, X., Jonker, M.T. and Hofmann, T. (2011) Measuring and modeling adsorption of PAHs to carbon nanotubes over a six order of magnitude wide concentration range. *Environ. Sci. Technol.* 45: 6011–6017.

Kavouras, I.G., DuBois, D.W., Nikolich, G. and Etyemezian, V. (2015). Monitoring, source identification and health risks of air toxics in Albuquerque, New Mexico, U.S.A. *Aerosol Air Qual. Res.* 15: 1160–1167.

Kim, K.H., Jahan, S.A., Kabir, E. and Brown, R.J.C. (2013). A review of airborne polycyclic aromatic hydrocarbons (PAHs) and their human health effects. *Environ. Int.* 60: 71–80.

Lai, Y.C., Huang, K.L., Tsai, C.H., Lee, W.J. and Chen, Y.L. (2012). Sputtered Pt loadings of membrane electrode assemblies in proton exchange membrane fuel cells. *Int. J. Energy Res.* 32: 918–927.

Lavall, R.L., Borges, R.S., Calado, H.D.R., Welter, C., Trigueiro, J.P.C., Rieumont, J., Neves, B.R.A. and Silva, G.G. (2008). Solid state double layer capacitor based on a polyether polymer electrolyte blend and nanostructured carbon black electrode composites. *J. Power Sources* 177: 652–659.

Lee, D. and Lee, D.G. (2016). Carbon composite bipolar plate for high-temperature proton exchange membrane fuel cells (HT-PEMFCs). *J. Power Sources* 327: 119–126.

Li, H., Liu, G. and Cao, Y. (2014). Content and distribution of trace elements and polycyclic aromatic hydrocarbons in fly ash from a coal-fired CHP plant. *Aerosol Air Qual. Res.* 14: 1179–1188.

Lin, C.C., Chen, S.J., Huang, K.L., Lee, W.J., Lin, W.Y., Tsai, J.H. and Chaung, H.C. (2008). PAHs, PAH-induced carcinogenic potency, and particle-extract-induced cytotoxicity of traffic-related nano/ultrafine particles. *Environ. Sci. Technol.* 42: 4229–4235.

Moninot, G. (2010). Where are the PAHs in the Carbon Black? www.iom3.org/fileproxy/331784, Last Access: Aug. 2015.

Mwangi, J.K., Lee, W.J., Tsai, J.H. and Wu, T.S. (2015). Emission reductions of nitrogen oxides, particulate matter and polycyclic aromatic hydrocarbons by using microalgae biodiesel, butanol and water in diesel engine. *Aerosol Air Qual. Res.* 15: 1160–1167.

Nisbet, C. and LaGoy, P. (1992). Toxic equivalency factors (TEFs) for polycyclic aromatic hydrocarbons (PAHs). *Regul. Toxicol. Pharm.* 16: 290–300.

Reshetenko, T., Serov, A., Artyushkova, K., Matanovic, I., Stariha, S. and Atanassov, P. (2016). Tolerance of non-platinum group metals cathodes proton exchange membrane fuel cells to air contaminants. *J. Power Sources* 324: 556–571.

Scofield, M.E., Liu, H. and Wong, S.S. (2015). A concise guide to sustainable PEMFCs: Recent Advances in improving both oxygen reduction catalysts and proton

exchange membranes. *Chem. Soc. Rev.* 44: 5836–5860.

Stogiannidis, E. and Laane, R. (2015). Source Characterization of Polycyclic Aromatic Hydrocarbons by Using Their Molecular Indices: An Overview of Possibilities, In *Reviews of Environmental Contamination and Toxicology*, Vol. 234, Whitacre, D.M. (Ed.), Springer International Publishing, Switzerland, pp. 49–133.

Tiwari, M., Sahu, S.K. and Pandit, G.G. (2015). Inhalation risk assessment of PAH exposure due to combustion aerosols generated from household fuels. *Aerosol Air Qual. Res.* 15: 582–590.

Tran, P.D., Morozan, A., Archambault, S., Heidkamp, J., Chenevier, P., Dau, H., Fontecave, M., Martinent, A., Jousselme B. and Artero, V. (2015). A noble metal-free proton-exchange membrane fuel cell based on bio-inspired molecular catalysts. *Chem. Sci.* 6: 2050–2053.

Tsai, J.H., Chen, S.J., Huang, K.L., Lin, T.C., Chaung, H.C., Chiu, C.H., Chiu, J.Y., Lin, C.C. and Tsai, P.Y. (2012). PM, carbon, PAH, and particle-extract-induced cytotoxicity emissions from a diesel generator fueled with waste-edible-oil-biodiesel. *Aerosol Air Qual. Res.* 12: 843–855.

Tsai, P.J., Shieh, H.Y., Hsieh, L.T. and Lee, W.J. (2001). The fate of PAHs in the carbon black manufacturing process. *Atmos. Environ.* 35: 3495–3501.

Wang, X., Zhang, H., Zhang, J., Xu, H., Zhu, X.B., Chen, J. and Yi, B.L. (2006). A bi-functional micro-porous layer with composite carbon black for PEM fuel cells. *J. Power Sources* 162: 474–479.

Wissler, M. (2006). Graphite and carbon powders for electrochemical applications. *J. Power Sources* 156: 142–150.

Zeis, R. (2015). Materials and characterization techniques for high-temperature polymer electrolyte membrane fuel cells. *Beilstein J. Nanotechnol.* 6: 68–83.

*Received for review, July 6, 2016*
*Revised, August 18, 2016*
*Accepted, August 19, 2016*